Physical modeling based on hydrodynamic simulation for the design of InGaAs/InP double heterojunction bipolar transistors*

Ge Ji(葛 霁)†, Liu Hong-Gang(刘洪刚), Su Yong-Bo(苏永波), Cao Yu-Xiong(曹玉雄), and Jin Zhi(金 智)

Key Laboratory of Microelectronics Device & Integrated Technology, Institute of Microelectronics, Chinese Academy of Sciences, Beijing 100029, *China*

(Received 6 October 2011; revised manuscript received 3 November 2011)

A physical model for scaling and optimizing InGaAs/InP double heterojunction bipolar transistors (DHBTs) based on hydrodynamic simulation is developed. The model is based on the hydrodynamic equation, which can accurately describe non-equilibrium conditions such as quasi-ballistic transport in the thin base and the velocity overshoot effect in the depleted collector. In addition, the model accounts for several physical effects such as bandgap narrowing, variable effective mass, and doping-dependent mobility at high fields. Good agreement between the measured and simulated values of cutoff frequency, $f_{\rm t}$, and maximum oscillation frequency, $f_{\rm max}$, are achieved for lateral and vertical device scalings. It is shown that the model in this paper is appropriate for downscaling and designing InGaAs/InP DHBTs.

Keywords: InGaAs/InP double heterojunction bipolar transistors, hydrodynamic simulation, lateral and vertical scalable model

PACS: 85.30.De, 73.40.Kp, 67.25.bf **DOI:** 10.1088/1674-1056/21/5/058501

1. Introduction

InGaAs/InP double heterojunction bipolar transistors (DHBTs) have been widely used to fabricate the power amplifiers working at the millimeter band and high speed mixed-signal integrated circuits due to their excellent material properties.[1,2] To achieve ultimate circuit operation, an InGaAs/InP DHBT with very high cutoff frequency, $f_{\rm t}$, and maximum oscillation frequency, $f_{\rm max}$, should be designed. An optimizing layer structure and downscaling geometric layout for high performance InGaAs/InP DHBTs is essential. From device design theory,[3] the use of a thin collector associated with a thin base can induce superior $f_{\rm t}$ and $f_{\rm max}$. In addition, the narrower emitter and collector junctions are able to operate the device at higher frequency. For this reason, a physical model for InGaAs/InP DHBTs, which can be efficiently and confidently used when downscaling and optimizing the device to achieve high $f_{\rm t}$ and $f_{\rm max}$, is required.

As the vertical dimensions of DHBT are reduced and the operation speed is increased, the transport of high-energy electrons can be significantly out of equilibrium, and the resulting velocity can be much higher than that in a steady state. Nonequilibrium electron transport in InGaAs/InP DHBTs becomes clearly observable, which cannot be accurately described by a conventional drift-diffusion model.[4] On the other hand, a Monte Carlo simulation of the device, which solves Boltzmann's transport equation,[5] can obtain accurate results. Unfortunately, because a Monte Carlo simulator computes the distribution of the electron energy at any device operation point, it is too time and memory consuming to simulate a device efficiently.

Currently, the most popular DHBT models, such as the Gummel–Poon or Agilent HBT models, are particularly suitable for fast circuit simulation. However, they are unscalable and cannot be used for device design, which must be calibrated with already fabricated and measured devices, and they cannot be used to analyse several physical effects such as bandgap narrowing, variable effective mass, carrier injection into the base and collector, as well as ballistic transport.

Therefore, in this paper, a physical model based on hydrodynamic simulation is used to analyse and assess the important physical effects and for the scaling

*Project supported by the National Basic Research Program of China (Grant No. 2010CB327502).

†Corresponding author. E-mail: imegeji@126.com

© 2012 Chinese Physical Society and IOP Publishing Ltd

and design of InGaAs/InP DHBTs. A hydrodynamic model taking electron heating and velocity overshoot effects into account can result in accurate results. In addition, a hydrodynamic model is simplified to compute only the average electron energy, which is much faster than the Monte Carlo simulator.

The rest of the paper is organized as follows. First, in Section 2, the structure of InGaAs/InP DHBTs is described. In Section 3, the physical hydrodynamic model is built in detail, including several physical effects, and in Section 4, we present the model that achieves good results when compared not only with the experimental data of a single device, but also with measurements of scaled versions of InGaAs/InP DHBTs.

2. The material and structure of InGaAs/InP DHBTs

In an InGaAs/InP DHBT, to eliminate the conduction band spike and suppress the current blocking effect, an InGaAsP composite collector is used.[6] The composite collector structure consists of an InGaAs setback layer and two step-graded InGaAsP layers. Figure 1 shows a typical cross-section of our fabricated InGaAs/InP DHBT structure. Due to device symmetry, only half the device needs to be simulated. In addition, the extrinsic collector is regarded as a parasitic part, which can be included in the model with the R–C network. When scaling the emitter width, the collector width is correspondingly scaled, keeping the base contact width and collector underetch unchanged, as depicted in Fig. 1. The layer structure of the InGaAs/InP DHBT is shown in Table 1, while the energy band diagrams of the device at thermal equilibrium are given in Fig. 2.

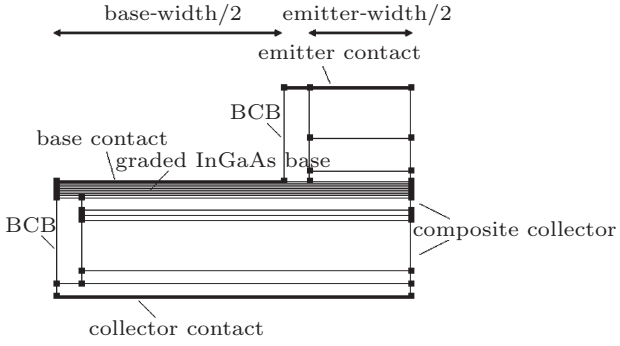


Fig. 1. Cross-section of our fabricated InGaAs/InP DHBT structure (BCB: benzocyclobutene).

Table 1. Simulated layer structure of the InGaAs/InP DHBT.

Layer	Material	Thickness/nm	Doping/cm^{-3}
emitter-cap	InGaAs	200	n:2×10^{19}
emitter	InP	130	n:1.2×10^{19}
emitter	InP	40	n:2×10^{17}
base	InGaAs	65	p:3×10^{19}
setback	InGaAs	50	n:1×10^{16}
grade	InGaAsP	20	n:1×10^{17}
grade	InGaAsP	20	n:1×10^{17}
collector	InP	200	n:1×10^{16}
collector	InP	50	n:1.2×10^{19}
sub-collector	InGaAs	50	n:2×10^{19}

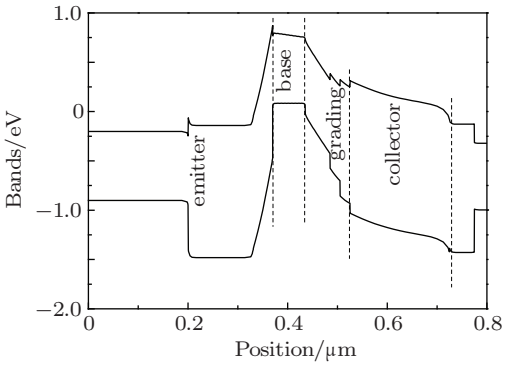


Fig. 2. Conduction and valence bands at zero bias of the InGaAs/InP DHBT.

3. Hydrodynamic model description

The electron model consists of the Poisson equation, continuity equations and energy conservation equations as follows:

$$\nabla \cdot \varepsilon \nabla \phi = -q(p - n + N_{\rm D} - N_{\rm A}) - \rho_{\rm trap}, \quad (1)$$

$$\boldsymbol{J}_{\rm n} = qu_{\rm n}(n\nabla E_{\rm C} + kT_{\rm n}\nabla n + kn\nabla T_{\rm n} - 1.5nkT_{\rm n}\nabla \ln m_{\rm n}), \quad (2)$$

$$\nabla \boldsymbol{S}_{\rm n} = \boldsymbol{J}_{\rm n} \cdot \nabla E_{\rm C} - n\frac{\partial w_{\rm n}}{\partial t} - n\frac{w_{\rm n} - w_0}{\tau_{\rm e}}, \quad (3)$$

$$\boldsymbol{S}_{\rm n} = -\frac{5r_{\rm n}}{2} \cdot \frac{kT_{\rm n}}{q}\boldsymbol{J}_{\rm n} - \frac{k^2}{q}nu_{\rm n}T_{\rm n}\Delta\nabla T_{\rm n}, \quad (4)$$

$$T_{\rm n} = gT_{\rm C} + (1 - g)T, \quad (5)$$

where ε is the electrical permittivity, ϕ is the electrostatic potential, q is the elementary electronic charge, n and p are the electron and the hole densities, $N_{\rm D}$ is the concentration of ionized donors, $N_{\rm A}$ is the concentration of ionized acceptors, $\rho_{\rm trap}$ is the charge density contributed by traps and fixed charges, $E_{\rm C}$ is the conduction band edge energy, T_n is the electron temperature, $m_{\rm n}$ is the electron effective masses, $\boldsymbol{S}_{\rm n}$ is the

energy flux, $w_{\rm n} = 3kT_{\rm n}/2$ is the average electron thermal energy, $w_0 = 3kT/2$ is the equilibrium thermal energy, $\tau_{\rm e}$ is the energy relaxation time, $r_{\rm n}$ is the energy flux parameter, Δ is the heat flux parameter, g is the thermal diffusion, $T_{\rm C}$ is the carrier temperature and T is the lattice temperature.

3.1. Mobility

As is well known, mobility is not only doping-related but also field-dependent.[7,8] For the hydrodynamic simulation, the electron mobility model is expressed by the following set of equations:

$$u_{\rm n,dop} = u_{\rm min} + \frac{u_{\rm d}}{1 + (N_{\rm dop}/N_0)^A}, \tag{6}$$

$$u_{\rm n,field} = \frac{u_{\rm n0} + \left(\frac{v_{\rm sat}}{E_0}\right)\left(\frac{F}{E_0}\right)^4}{1 + \left(\frac{F}{E_0}\right)^4}, \tag{7}$$

$$\frac{1}{u_{\rm n}} = \frac{1}{u_{\rm n,dop}} + \frac{1}{u_{\rm n,field}} - \frac{1}{u_{\rm n0}}, \tag{8}$$

where F is the driving force; $N_{\rm dop}$ is the doping concentration; $u_{\rm d}$, N_0, and A are temperature-dependent coefficients; $v_{\rm sat}$, $u_{\rm min}$, and E_0 are cited from Refs. [7], [9], and [10]; $u_{\rm n0}$ is the low field mobility at low doping; $u_{\rm n,dop}$ is the mobility due to impurity scattering, and $u_{\rm n,filed}$ is the field-dependent mobility at low doping. Then, the electron mobility can be obtained by Eq. (8).

The driving force for the electron is

$$F = \sqrt{\frac{w_{\rm n} - w_0}{q u_{\rm n} \tau_{\rm e}}}. \tag{9}$$

3.2. The physical properties of the model

For InGaAs/InP DHBTs, there are additional physical effects to be included in the physical model.

3.2.1. Thermionic emission

At a general forward emitter-base bias, thermionic emission is a dominant effect for InGaAs/InP DHBTs. The thermionic emission equation system for electrons can be written as

$$J_{\rm n,E} = J_{\rm n,B}, \tag{10}$$

$$J_{\rm n,E} = aq\left[v_{\rm n,E} n_{\rm E} - \frac{m_{\rm e,E}}{m_{\rm e,B}} v_{\rm n,B} n_{\rm B} \exp\left(-\frac{\Delta E_{\rm C}}{kT_{\rm n,B}}\right)\right], \tag{11}$$

$$S_{\rm n,E} = S_{\rm n,B} + \frac{c}{q} J_{\rm n,E} \Delta E_{\rm C}, \tag{12}$$

$$S_{\rm n,E} = -bk_{\rm B}\left[v_{\rm n,E} n_E T_{\rm n,E} - \frac{m_{\rm e,E}}{m_{\rm e,B}} v_{\rm n,B} n_{\rm B} T_{\rm n,B} \exp\left(-\frac{\Delta E_{\rm C}}{kT_{\rm n,B}}\right)\right], \tag{13}$$

where the emission velocity is defined as

$$v_{\rm n,i} = \sqrt{\frac{k_{\rm B} T_{\rm n,i}}{2\pi m_{\rm e,i}}}, \tag{14}$$

with the subscripts 'E' and 'B' denoting the emitter and base, respectively; $J_{\rm n,i}$ and $S_{\rm n,i}$ are the current density and the energy flux density with i=E or B, respectively; parameters a, b, and c are extracted from the measurements for the bias point where the Kirk effect takes place.

3.2.2. Bandgap narrowing

It is important to simulate bandgap narrowing due to heavy doping.[9] If bandgap narrowing is ignored, the energy band diagrams will be distorted and electron transport across potential barriers such as base-emitter junctions will be blocked. As a result, the current gain and the cutoff frequency are much lower than the actual values. Therefore, bandgap narrowings are implemented for all heavily doped layers in the model. Bandgap narrowing is most pronounced in the highly doped base where the bandgap reduces 75 meV.[9,11]

3.2.3. Doping-dependent effective mass

In general, physics-based device simulators use a simple parabolic band model, and restrict the effective mass to a constant quantity. However, this is only an accurate approximation near the conduction band minimum or valence band maximum. If $N_{\rm D}$ and $N_{\rm A}$ become comparable to or greater than the conduction band density of states ($N_{\rm C}$) and valence band density of states ($N_{\rm V}$), the Fermi-level ($E_{\rm F}$) enters into the conduction or valence band. The energy level occupied by the carrier is higher than the band minimum. The constant effective mass cannot properly account for the properties of the degenerately doped semiconductors. In this paper, a third polynomial equation is used to represent the electron effective mass.[9]

3.2.4. Surface traps

Missing atoms at the surface produce traps which can generate recombination current. Surface traps

with surface densities and energy levels as given in Ref. [12] have been incorporated into the model.

3.2.5. Recombination

Shockley–Read–Hall (SRH), radiative and Auger recombination values from the literature have been incorporated into our model: $\tau_{\rm SRH} = 60$ ns, $C_{\rm rad} = 1.4\times10^{-9}$ cm^3/s, and $C_{\rm Auger} = 4\times10^{-29}$ cm^6/s. The radiative recombination in the base is a dominant bulk recombination effect.

3.2.6. Contact resistances

The contact resistance which can be concluded from the transmission-line measurement has been used in our model: the specific contact resistance of the emitter contact ($\rho_{\rm E}$) is 3×10^{-7} $\Omega\cdot$cm^2, the specific contact resistance of the base contact ($\rho_{\rm B}$) is 2×10^{-7} $\Omega\cdot$cm^2, and the specific contact resistance of the collector contact ($\rho_{\rm C}$) is 3×10^{-7} $\Omega\cdot$cm^2.

3.2.7. External resistance and parasitic capacitance

The external emitter and collector resistances, base-emitter and collector-emitter parasitic capacitances can be extracted from a small-signal model for the devices.[13]

4. Hydrodynamic model verification of laterally and vertically scaled DHBTs

In this section, the model is verified by comparing with experimental or reported data for laterally and vertically scaled DHBTs. The simulation is consistent with the results from the scaling theory and experiment.

4.1. Base and collector transit times

The cutoff frequency $f_{\rm t}$ is related to the emitter-collector transit time ($\tau_{\rm EC}$) as follows:

$$\frac{1}{2\pi f_{\rm t}} = \tau_{\rm EC} = \frac{\eta kT}{qI_{\rm E}}(C_{\rm BE}+C_{\rm BC}) + C_{\rm BC}(R_{\rm E}+R_{\rm C}) + \tau_{\rm B} + \tau_{\rm C}. \quad (15)$$

For a modern InGaAs/InP DHBT, the base transit time of $\tau_{\rm B}$ and the collector transit time of $\tau_{\rm C}$ are becoming dominant terms in this sum. In order to enhance the high-speed operation of DHBT, the reductions of $\tau_{\rm B}$ and $\tau_{\rm C}$ are essential, which is the main reason for a vertical downscaling InGaAs/InP DHBT. The strongly effective verification of the model is to simulate and predict the rules of $\tau_{\rm B}$ and $\tau_{\rm C}$ that vary with device thickness.

The values of $\tau_{\rm B}$ and $\tau_{\rm C}$ can be obtained using the following formulas:[4,14]

$$\tau_{\rm B} = \int_0^{d_{\rm B}} \frac{{\rm d}x}{v(x)}, \quad (16)$$

and

$$\tau_{\rm C} = \int_0^{d_{\rm C}} \frac{{\rm d}x}{v(x)}\left(1-\frac{x}{d_{\rm C}}\right), \quad (17)$$

where $v(x)$ is the carrier velocity, and $d_{\rm B}$ and $d_{\rm C}$ are the base thickness and the collector thickness. According to the equation, $v(x)$ should be simulated to obtain the $\tau_{\rm B}$ and $\tau_{\rm C}$ values of InGaAs/InP DHBTs. Figure 3 shows the velocity profiles obtained by our model for a bias point with a high current density at which the Kirk effect takes place. Our results are similar to the Monte Carlo simulation results.[4]

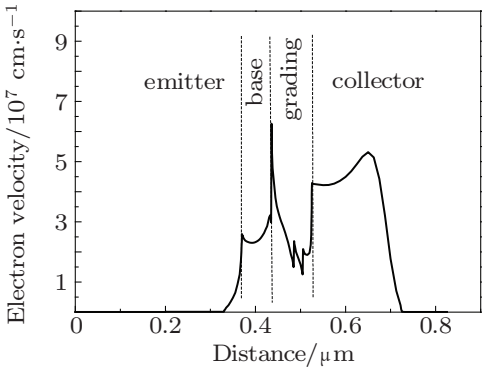


Fig. 3. Electron velocity profiles in InGaAs/InP DHBTs obtained by hydrodynamic simulation.

First, in a DHBT with abrupt emitter/base interface, when electrons are injected from the emitter barrier into the base, the initial velocity yield by the conduction band discontinuity $\Delta E_{\rm C}$ can be high (Fig. 3). Then, in the base, the scattering rate can be much higher by an accumulation of quasi-thermalized carriers due to the electron with a randomized velocity vector.[4] In order to solve this problem, a graded base is designed which can sweep out quasi-thermalized carriers and speed the electrons. Next, in the grading layer, the electron velocity overshoot appears (Fig. 3). However, the energy loss of electrons through inelastic scattering is high due to the very high field.[4,15] As a result, the overshoot width is narrow and the electron velocity shrinks quickly. Finally, in the collector,

$\Delta E_{\Gamma-L}$ is 0.6 eV in InP and the field is low, which promises a much wider overshoot range compared with that in the grading layer. The quasi-ballistic transport appears over a large fraction of the collector layer, and electron velocities higher than 4×10^7 cm/s are maintained, as shown in Fig. 3.

The reasonable agreement between the simulated and measured data for the base and the collector transit times is important for the verification of the model. Figure 4 shows that the model-based calculated and experimental data for the overall transit $\tau_B+\tau_C$, each as a function of base thickness d_B, are in good agreement.[4,16] It can be seen that τ_B changes as $\tau_B \propto d_B^2$ for d_B, ranging from 20 to 100 nm, where the classical diffusive transport of electrons takes place, and as $\tau_B \propto d_B$ for d_B less than 20 nm, which is indicative of ballistic transport. The phenomenon is in agreement with the result in Ref. [4]. Figures 5(a) and 5(b) show the plots of $\tau_B+\tau_C$ (reported measurements and calculations in this model) as a function of d_B+d_C.[16–20] The deviation is consistently less than 10%.

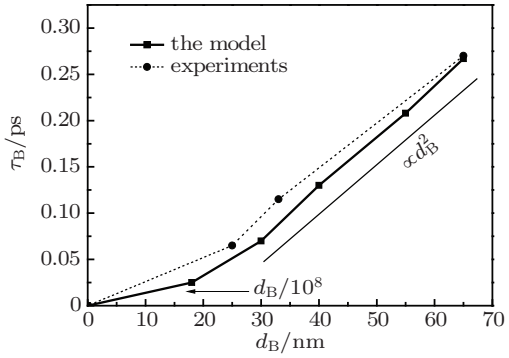


Fig. 4. Measured and model-based calculated τ_B versus d_B for InGaAs/InP DHBTs.

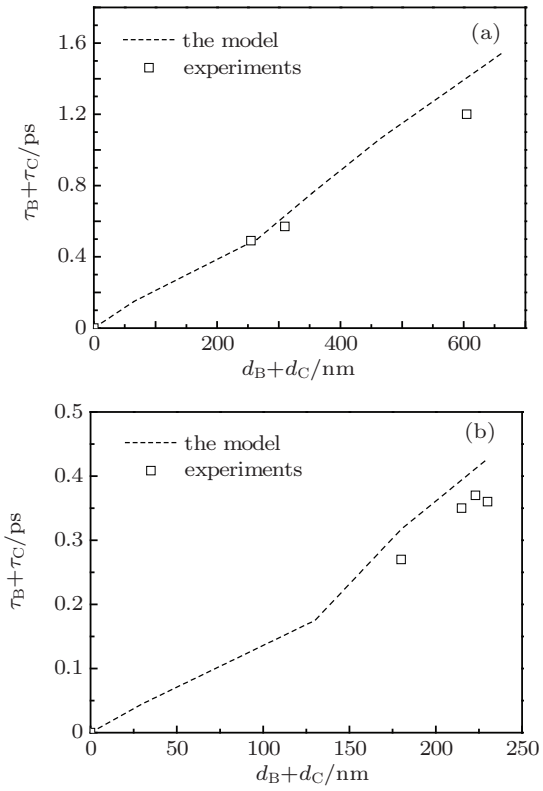


Fig. 5. The sum of base and collector thickness $d_B + d_C$ versus $\tau_B + \tau_C$. (a) d_B = 50–65 nm, (b) d_B = 25–33 nm.

4.2. High-frequency performance

The most important figures of merit characterizing the high-frequency performance of DHBT are f_t and f_{max}. Therefore, the most important aspect of

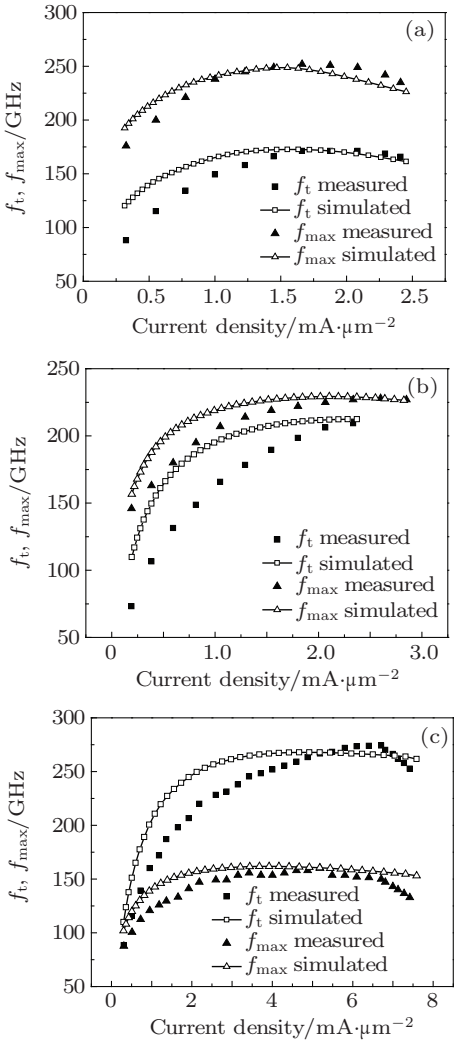


Fig. 6. Measured and model-based calculated f_t and f_{max} values for InGaAs/InP DHBTs with different values of d_B, d_C, and A_E: (a) d_B = 65 nm, d_C = 290 nm, and $A_E = 1\times14$ μm^2; (b) d_B = 40 nm, d_C = 200 nm, and $A_E = 1\times14$ μm^2; (c) d_B = 30 nm, d_C = 100 nm, and $A_E = 0.7\times20$ μm^2.

the model is to correctly estimate the f_t and f_{max} values of InGaAs/InP DHBTs. Figure 6 shows the values of f_t and f_{max} versus current density for InGaAs/InP DHBTs with different values of d_B, d_C, and an active emitter area A_E. The Kirk current point, at which the maximum f_t is measured, depends on the layer structure design, contact resistances, fabrication process, and test accuracy, which cannot be simulated very accurately by numerical simulation before the device is fabricated. The deviation in model-based calculated values is always smaller than 20% compared with those of the measurements. The accuracy of the model is suited to downscaling and optimizing the structure of InGaAs/InP DHBTs.

5. Conclusion

In maximizing InGaAs/InP DHBT performance for circuit applications, there are two tradeoffs, f_t versus R_B and R_E in the lateral direction and f_t versus C_{BC} in the vertical direction. The narrower emitter can improve f_t but increase R_B and R_E, which leads to low f_{max}. The reduction in collector thickness can reduce τ_{EC} but increase C_{BC} and lower the breakdown voltage. The actual design optimization of InGaAs/InP DHBTs is not simple because many parameters must be taken into account. There is a strong requirement for the model to scale and optimize the layer structure of InGaAs/InP DHBTs, which cannot be achieved by the currently most popular model. The model presented in this paper can meet the requirement and be used to design high performance InGaAs/InP DHBTs for circuit applications.

References

[1] Hacker J, Urteaga M, Mensa D, Pierson R, Jones M, Griffith Z and Rodwell M 2008 *IEEE MTT-S Int. Dig.* Atlanta, USA, June 15–20, 2008 p. 403

[2] Griffith Z, Urteaga M, Pierson R, Patane A, Rodwell P, Rodwell M and Brar B 2010 *IEEE Compound Semiconductor Integrated Circuit Symposium* Costa Mesa, USA, October 3–6, 2010 p. 1

[3] Rodwell M J W, Urteaga M, Mathew T, Scott D, Mensa D, Lee Q, Guthrie J, Betser Y, Martin S C, Smith R P, Jaganathan S, Krishnan S, Long S I, Pullela R, Agarwal B, Bhattacharya U, Samoska L and Dahlstrom M 2001 *IEEE Trans. Electron Devices* **48** 2606

[4] Ishibashi T 2001 *IEEE Trans. Electron Devices* **48** 2595

[5] Kazutaka T 1993 *Numerical Simulation of Submicron Semiconductor Devices* 1st ed (Norwood: Artech House)

[6] Jin Z, Su Y B, Cheng W, Liu X Y, Xu A H and Qi M 2009 *Chin. Phys. Lett.* **25** 2686

[7] Caughey D M and Thomas R E 1967 *Proc. IEEE* **55** 2192

[8] Lv H L, Zhang Y M and Zhang Y M 2004 *Chin. Phys.* **13** 1100

[9] Li J C, Sokolich M, Hussain T and Asbeck P M 2006 *Solid-State Electronics* **50** 1440

[10] Tauqeer T, Sexton J, Amir F and Missous M 2008 *International Conference on Advanced Semiconductor Devices and Microsystems* Smolenice, Slovakia, October 12–16, 2008 p. 271

[11] Lopez-Gonzalez J M and Part L 1997 *IEEE Trans. Electron Devices* **44** 1046

[12] Ruiz-Palmero J M, Hammer U and Jackel H 2006 *Solid-State Electronics* **50** 1595

[13] Ge J, Jin Z, Su Y B, Cheng W, Liu X Y and Wu D X 2009 *Acta Phys. Sin.* **58** 8584 (in Chinese)

[14] Blayac S, Benchimol J L, Abboun M, Aniel F, Berdaguer P, Duchenois A M, Konczykowska and Godin J 1999 11*th International Conference on Indium Phosphide and Related Materials* Davos, Switzerland May 16–20, 1999 p. 483

[15] Guo B Z, Zhang S L and Liu X 2011 *Acta Phys. Sin.* **60** 068701 (in Chinese)

[16] Kahn M, Blayac S, Riet M, Berdagaguer P, Dhalluim, Alexandre F and Godin J 2003 *IEEE Electron Dev. Lett.* **24** 430

[17] Willen B, Westergren U and Asonen H 1995 *IEEE Electron Dev. Lett.* **16** 479

[18] Kurishima K, Nakajima H, Kobayashi T, Matsuoka Y and Ishibashi T 1993 *Electronics Lett.* **29** 258

[19] Ida M, Kurishima K, Ishii K and Watanabe N 2003 *Gallium Arsenide Integeated Circuit Symposium: Technical Digest* San Diego, California November 9–12, 2003 p. 211

[20] Ida M, Kurishima K, Watanabe N and Enoki T 2001 *Electron Devices Meeting* Washington, D. C. December 2–5, 2001 p. 35.4.1